IEEE Access
Multidisciplinary ⋮ Rapid Review ⋮ Open Access Journal

Received 18 March 2023, accepted 8 April 2023, date of publication 12 April 2023, date of current version 20 April 2023.

Digital Object Identifier 10.1109/ACCESS.2023.3266649

RESEARCH ARTICLE

Beam Shaping of Base Station Antenna Array by Using MMPTE

LIN GUO[1], SHEN-YUN WANG[2], (Member, IEEE), GUO-WEN DING[2], (Member, IEEE), AND WEN GEYI[2]

[1]School of Electronic and Information Engineering, Nanjing University of Information Science and Technology, Nanjing 210044, China
[2]Research Center of Applied Electromagnetics, Nanjing University of Information Science and Technology, Nanjing 210044, China

Corresponding author: Shen-Yun Wang (wangsy2006@126.com)

This work was supported in part by the National Natural Science Foundation of China under Grant 61971231, and in part by the Natural Science Foundation of Jiangsu Province of China under Grant BK20220440.

ABSTRACT In this paper, a beam shaping scheme is presented for the optimal design of base station antenna array. The antenna array consists of four linearly arranged dual-band dual-polarized antenna elements, and it is designed to cover the LTE frequency band (2.3-2.69 GHz) and 5G frequency band (3.3-3.6 GHz). The shaped beams with possible maximum gain, suppressed sidelobe level smaller than −16 dB, front-to-back ratio larger than 18dB, and filled-up null point larger than −23 dB are accomplished through two steps by using the unconstrained methods of maximum power transmission efficiency (MMPET) and constrained MMPTE, respectively. In the proposed beam shaping scheme, all the realistic factors of the antenna array have been taken into account, such as the difference of element radiation patterns, complexity and tolerance of the element structure and spacing.

INDEX TERMS Base station antenna array, beam shaping, MMPTE, sidelobe, null point.

I. INTRODUCTION

Starting from 2019, the fifth generation (5G) mobile communication system enters the commercial era. Mobile communication networks organize the service area into geographically separated zones, known as cells, so as to execute the frequency reuse strategy and to increase the throughput capacity of the system, where the frequency bandwidth and shaped radiation pattern of the base station antenna array play two important roles [1].

Although the 5G communication has been in commercial use, the 4G, 3G, or even 2G systems are expected to be in service for a long time. For saving the cost and space of the base station, broadband or multiband antenna array is widely investigated for base station [2], [3], [4], [5], [6], [7], [8], [9], [10]. To reduce the side effect of the multipath fading and to enhance signal reliability, dual-polarized antenna elements are widely investigated for the base station antenna array [11], [12], [13], [14], [15], [16]. Hence, broadband or multiband dual-polarized base station antenna arrays have been heavily researched in recent years.

Although multiple frequency bands have been authorized for the mobile communication systems, the insufficiency of channel is still a serious problem because of the increase of user ends (UEs) and the demand for large capacity, which requires more efficient frequency reuse. For this reason, the cell size of the 5G cellular mobile system tends to be smaller. In this case, the antenna array of base station is required to have a shaped radiation beam that must satisfy some basic conditions: First, the sidelobe level (SLL) pointing to anther cell or the black-lobe pointing to another sector that works at the same frequency must be as low as possible in order to reduce the co-channel interference; Second, the main beam of the pattern has to provide the maximum possible gain $G(\theta_{max})$ at the desired direction determined in the spherical coordinate system; Third, for a fixed network, the ideal shaped beam pattern for a planar service cell is usually a cosecant squared pattern. In practice, pattern nulls pointing to service cell should be filled up, so as to avoid blind communication zones.

Many beam shaping techniques have been suggested for the design of antenna arrays in order to produce desired

The associate editor coordinating the review of this manuscript and approving it for publication was Debdeep Sarkar.

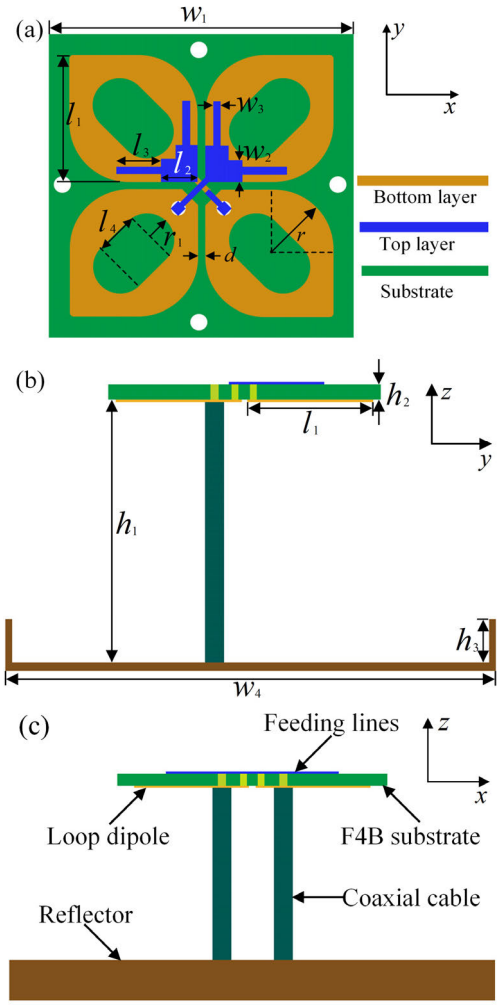

FIGURE 1. Configuration of the antenna element: (a) loop dipole radiator, (b) front view, and (c) side view.

radiation patterns for specific applications [17], [18], [19], [20], [21], [22], [23], [24], [25], [26], [27], [28]. Some traditional pattern synthesis methods, such as Taylor and Chebyshev methods [17], [18], are used to suppress the SLL of antenna arrays. To realize more complex shaped beam patterns of antenna array, global/local iterative optimization schemes, such as genetic algorithm (GA) [19], [20], particle swarm optimization (PSO) [1], [21], [22], convex optimization (CO) [23], [24] and sampling/superposition methods [25], [26], [28], have been reported to shape a desired beam pattern. However, most of the array synthesis methods are based on the pattern multiplication rule that ignores the differences of radiation patterns of antenna elements, the mutual-coupling, and the influence of the antenna mounting-platform. In practice, the mutual-coupling and patterns may be different among the array elements locating at different zones in the array. When the array element is assumed to be a point source, the array synthesis can be oversimplified to optimize the array factor. For the synthesis of a realistic antenna array, the pattern multiplication rule demands identical element radiation pattern, and the element factor should be extracted at first, so the synthesizing pattern can be written in terms of trigonometric polynomials. However, it fails when the element patterns are of no longer unity, or the surrounding environment is too complicated. For the global optimization methods, if the fitness function includes all the array effecting factors [22], the optimization process will become computationally cumbersome.

In this paper, a beam shaping scheme is proposed by using the unconstrained method of maximum power transmission efficiency (U-MMPTE) [29], [30], [31] and constrained method of maximum power transmission efficiency (C-MMPTE) [32], [33]. The proposed beam shaping method is valid for any realistic antenna array in regardless of the difference of the element pattern, complexity of the antenna configuration, the surrounding environment, and difference of the mutual coupling among the array elements. Hence, a dual-band dual-polarized base station antenna array is designed and fabricated, and its beam patterns with desired main beam direction, suppressed sidelobe level and filled-up null point are shaped through the beam shaping method. The shaped beam patterns meet the base station standards for LTE and 5G communication systems.

The structure of this paper is organized as follows. After the introduction in Section I, the configuration of the base station antenna and beam shaping scheme are described in Section II. Section III describes the simulated and measured results of the shaped beams for base station antenna array. Section IV draws the conclusions.

II. ANTENNA AND PATTERN SYNTHESIS METHOD

To demonstrate the beam shaping scheme on a realistic antenna array, at first a dual-band dual-polarization based station antenna array is designed and fabricated.

A. CONFIGURATION OF ANTENNA ELEMENT

The geometry of the designed dual-polarized antenna element is illustrated in Fig.1. It consists of a metal gutter reflector, a pair of loop dipoles, Y-shaped feeding lines, and a pair of coaxial cables. As shown in Fig.1(a), a pair of mutually orthogonal loop dipoles are printed on the bottom of an F4B dielectric substrate with dielectric constant of 2.55, loss tangent of 0.0015, and thickness of 0.8 mm, and the Y-shaped feeding lines are printed on the top of the F4B substrate. To prevent the two feed lines from intersection, the overlapping part of one Y-shaped feed line is printed on the bottom face of the F4B substrate and connected to the top parts with two metalized vias. Both loop radiator dipoles are fed by a 50-ohm coaxial cable, where the inner conductors are connected to the Y-shaped feeding lines and the outer conductors are soldered on the loop radiators, as shown in Figs. 1(b) and (c). To make the inner conductors connect to the feeding lines, two more holes are drilled through the F4B substrate.

TABLE 1. Parameters of the designed antenna (units: mm).

Parameters	Value	Parameters	Value
l_4	5	l_1	20
r_1	4	l_2	5.5
d	1	l_3	6.5
r	9	w_1	45
h_1	26	w_2	3.5
h_2	0.8	w_3	1
h_3	10	w_4	90

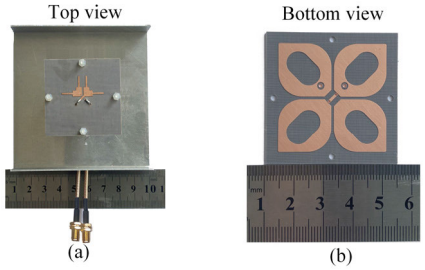

FIGURE 2. Photo of the antenna element. (a) Top view of the antenna element, and (b) bottom view of the loop dipole radiators.

The RF signal is fed to the Y-shaped feeding lines through the coaxial cable, and the RF energy is coupled to the loop dipole through the Y-shaped feeding line, which results in a symmetrical feeding. Modifying the size and position of the Y-shaped feeder can enhance the coupling strength, so as to improve the bandwidth and impedance matching.

Many efforts have been devoted to developing antennas in the 3.5 GHz band for 5G communication. However, the frequency bands for 2G/3G/LTE communication systems still co-exist with the granted 5G frequency band. In this work, an antenna element for both 5G band covering 3.3-3.6 GHz and an LTE band covering 2.3-2.69 GHz is optimized. The optimized parameters are listed in Table 1. Compared with the traditional wire dipoles, the loop radiator dipoles have a widened impedance bandwidth.

To verify the proposed design, a prototype of the designed dual-band dual-polarized antenna element is fabricated and tested. The top view of the antenna element and bottom side of the F4B substrate together with the printed loop dipoles are shown in Figs.2 (a) and (b), respectively, and the principal substrate is supported by four nylon columns.

Due to the symmetry of the dual-port antenna element, only one of the feeding ports is excited to validate the performance of the antenna element working in 2-4GHz. The reflection coefficient ($|S_{11}|$) and port-to-port isolation ($|S_{21}|$) is plotted in Fig. 3. It is observed that the measured −15 dB impedance matching bandwidths are 2.3-2.8 GHz, and 3.2-3.8 GHz, which cover the LTE band and 5G band, respectively, and agree well with the simulated results. The simulated and measured port-to-port isolation is less than −17 dB in 2-4GHz band. The measured and simulated peak gain of the antenna

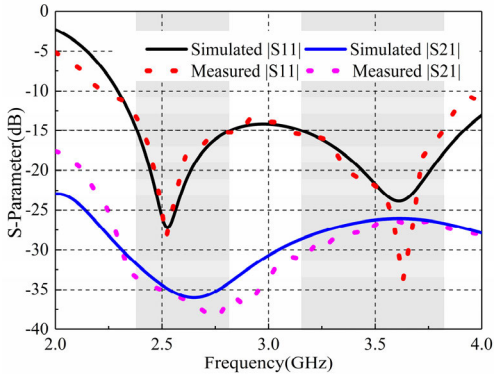

FIGURE 3. S-parameters of the antenna element.

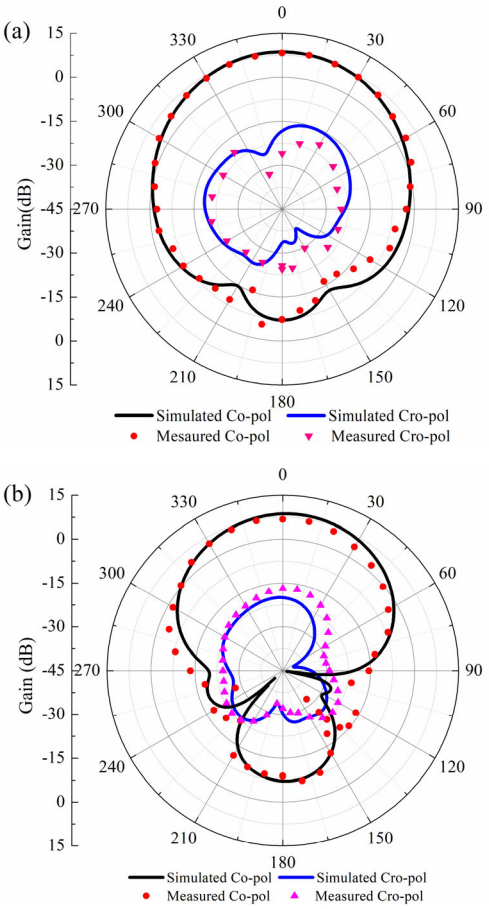

FIGURE 4. Gain pattern of the antenna element on the (a) E-plane and (b) H-plane.

element in the main radiation direction is 8.57 dB, and the maximum cross-polarization gain level is below −16 dB in E-plane (+45°) and below −19 dB in H-plane (−45°), and the cross-polarization ratio in ±60° is greater than 17 dB, and the half-power beamwidth (HPBW) in E-plane and H-plane is about 68° ± 5°, as shown in Figs. 4 (a) and (b). The radiation efficiency of the antenna element is 78.79% at 3.0 GHz, 76.37% at 2.45 GHz and 78.43% at 3.5 GHz.

FIGURE 5. Photo of four-element antenna array.

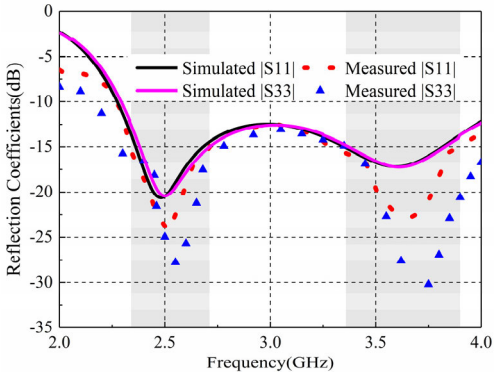

FIGURE 6. Simulated and measured reflection coefficients of the antenna array elements.

B. CONFIGURATION OF ANTENNA ARRAY

To better describe the beam shaping of the antenna array, the *xoz*-plane is defined as the horizontal plane and the *yoz*-plane is treated as the vertical plane. For practical base station application in a cellular mobile communication system, the antenna demands a narrow radiation pattern in vertical plane, a stable radiation pattern in horizontal plane (-3dB beamwidth of $65° \pm 5°$, which is mainly determined by the antenna element and the metal reflector), a down tilt of the antenna beam with suppressed sidelobe level and large front-to-back ratio to reduce the interference in the other co-channel cells or sectors, and a filled-up null point in the service cell to avoid blind spot. To achieve all of the required antenna performances, an antenna array is required. On the basis of antenna element design, a prototype of four-element antenna array is fabricated, as illustrated in Fig.5. Selecting the beam shaping at 2.45GHz and 3.5GHz within the two interesting bands, a compromising element spacing is set to be 50 mm (about $0.57\lambda_{3.4\text{GHz}}$ and $0.41\lambda_{2.45\text{GHz}}$) for preventing grating-lobe in the upper frequency band, and the total length of the four-element antenna array in vertical direction is 385mm. To validate the performance of the four-element antenna array, the impedance matching bandwidth is simulated and measured as shown in Fig.6. It can be found that both the simulated and measured impedance matching bandwidth cover LTE band (2.3-2.69 GHz) and 5G band (3.3-3.6 GHz), and slight impedance matching difference occurs between the edge element ($|S_{11}|$ or $|S_{44}|$) and middle element ($|S_{22}|$ or $|S_{33}|$).

C. BEAM SHAPING METHOD

Traditional beam shaping methods usually rely on certain simplifications in order to reduce the complexity of the optimization process. However, the simplifications may cause significant error when the array element patterns are not identical, or the mounting-platform of the antenna array is too complicated, and/or the element spacing is very small. In this work, the U-MMPTE and C-MMPET is used to shape the beam patterns of the four-element antenna array for base station application. Beam patterns with different down-tilt angles, suppressed sidelobe level smaller than -16 dB, front-to-back ratio larger than 18 dB and filled-up null point larger than -23 dB are shaped through two steps by using U-MMPTE and C-MMPET, respectively.

In the first step, the goal is to realize the main beam in a desired direction and confirm the concomitant side lobes and null points pointing to the service cell. To achieve this goal, a testing antenna of matched operating frequency and polarization is introduced on the far-field arc in each discreted elevation directions. The first WPT system is built up by selecting the testing antenna in desired direction (Rx1) as sketched in Fig.9. The power transmission efficiency (PTE) between the transmitting (Tx) antenna array and the testing antenna as the receiving (Rx) antenna is defined as the ratio of the power (P_{rec}) delivered to the load of the receiver to the input power (P_{in}) of the transmitting antenna array [33]:

$$PTE = \frac{P_{\text{rec}}}{P_{\text{in}}} = \frac{\langle [A]\,[a_t]\,,[a_t]\rangle}{\langle [a_t]\,,[a_t]\rangle} \tag{1}$$

where $[A] = [S_{rt}]^H [S_{rt}]$ is determined by the simulated or measured scattering parameters, and $[a_t] = [a_1, \cdots, a_N]^T$ is the normalized excitation vector of the transmitting antenna elements. To direct the main beam toward to the direction of the testing antenna, the PTE has to be maximized and a generalized algebraic eigenvalue equation is obtained [33]:

$$[A]\,[a_t] = PTE \cdot [a_t] \tag{2}$$

The maximum eigenvalue gives the maximum PTE and the corresponding eigenvector stands for the ODEs of the transmitting antenna array.

In the second step, the goal is to suppress the upper side lobe level and to fill up the null point within the service cell while maximumly keeping the main beam direction and radiation gain unchanged. To realize this goal, additional two testing antennas (Rx2 and Rx3 marked in blue in Fig.9) in the side lobe and null point directions are selected to build up the second WPT system. Due to the front-to-back ratio or back side lobe is mainly controlled by the configuration of the metal reflector for co-linear antenna array, the additional testing antennas are selected to control the upper side lobe levels and lower null points. To suppress the upper side lobe levels and lower null points based on the second WPT

system, the beam shaping leads to a constrained optimization problem [33]:

$$\max \langle [A]\,[a_t]\,,\,[a_t]\rangle$$
$$\text{s.t.}\,[b_r] = [S_{rt}]\,[a_t] = [c]\,e^{j\varphi} \tag{3}$$

where $[b_r] = [b_1, \cdots, b_M]^T$ is the reflecting wave vector of the test receiving antennas. Here, the phase difference among the Rx antennas is negligible due to that the testing antenna is placed on a far-field arc to extract the S-parameters for the case of multiple Rx antennas, and the constrained optimization problem becomes a linearly constrained programing problem. Moreover, the exponential term in (3) can be factored in the excitation vector $[a_t]$. By using the method of Lagrangian multiplier, the optimized solution of (3) is given by [33]:

$$[a_t] = [A]^{-1}\,[S_{rt}]^H \left([S_{rt}]\,[A]^{-1}\,[S_{rt}]^H\right)[c] \tag{4}$$

In order to suppress the first upper sidelobe and to fill up the first lower null point, one can properly set up the controlling vector $[c] = [c_{\text{SLL}}, c_{\text{Max}}, c_{\text{NULL}}]$. For the best suppression of the first upper sidelobe level, c_{SLL} is usually set to be zero and the rest two controlling weights should satisfy $c_{\text{Max}} > c_{\text{NULL}}$, so as to maintain a maximum possible gain of the main beam when suppressing the upper sidelobe level and filling up the lower null point. For a large-scale antenna array, more testing antennas may be introduced to control the multiple sidelobes and null points, and more accurate beam pattern can be shaped.

D. FEEDING CIRCUIT

To realize a reconfigurable excitation of the fabricated four-element antenna array, a four-channel RF feeding network is designed to provide the driving phase and amplitude obtained from the beam shaping method. The schematic and the photo of the feeding network are shown in Figs.7(a) and (b), respectively. The input RF signal is equally divided into the four channels through a 4-way power divider. In each channel, a low-cost analog phase shifter (PS) and attenuator (ATT) are used to adjust the output phase and the amplitude. The analog PS and ATT can be continuously controlled through bias-voltage by adjusting the rheostat on the voltage regulator circuit. The input DC-voltage is 9V, and the output bias-voltages ($V_{ai}, i = 1, \cdots, 4$) for the ATTs range from 0 to 9V, resulting in 0-31.5dB attenuation for the driving signal at 2.45GHz; and the output bias-voltages ($V_{pi}, i = 1, \cdots, 4$) for the phase shifters vary from 2.5 to 15V, resulting in 0-360° phase shift for 2.45GHz RF signal. The rheostats on the voltage regulator circuits can be continuously adjusted, and therefore the output phases and amplitudes of the feeding network are of high precision. The insertion loss of the transmission line is included in the total attenuation of each channel in the calibration stage.

As shown in Fig. 8, the antenna array system consists of a RF signal generator, the four-channel feeding network, and the four-element antenna array, and they are properly

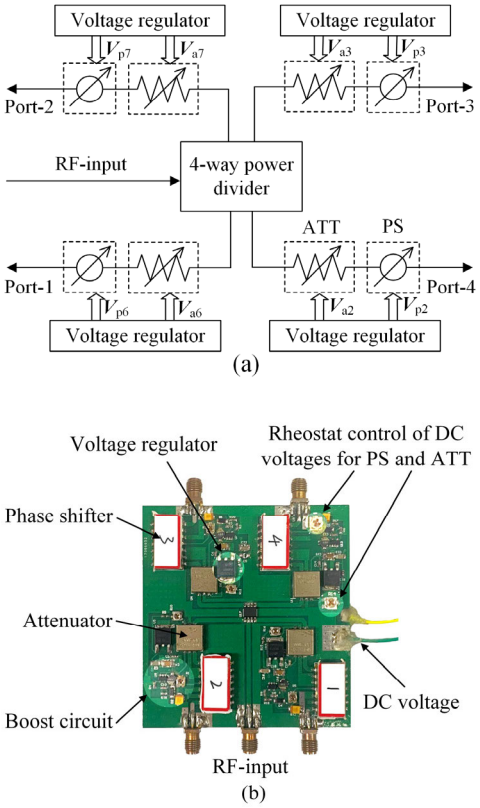

FIGURE 7. The feeding circuit: (a) circuit schematic, (b) photo.

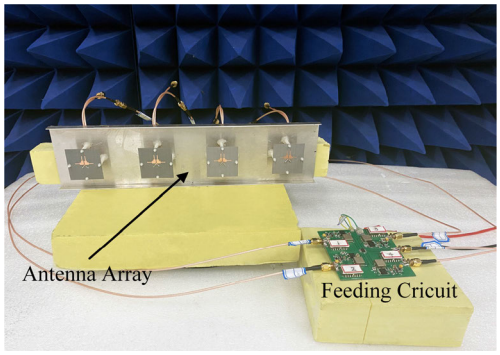

FIGURE 8. Photo of the proposed antenna array system.

connected by coaxial cables. A 9V DC-voltage source is also used to provide the bias-voltage of the feeding network. The input power of the feeding circuit is 13dBm from a RF generator, and the attenuation of each channel refers to that of the channel providing the largest signal amplitude. The total output power of the feeding circuit is test through a frequency spectrograph for calculating the gain of the antenna array. Finally, the radiation pattern of the antenna system is tested in a microwave anechoic chamber.

III. RESULTS AND DISSCUSSIONS

The beam shaping in the horizontal plane for a co-linear antenna array is mainly determined by the configuration of

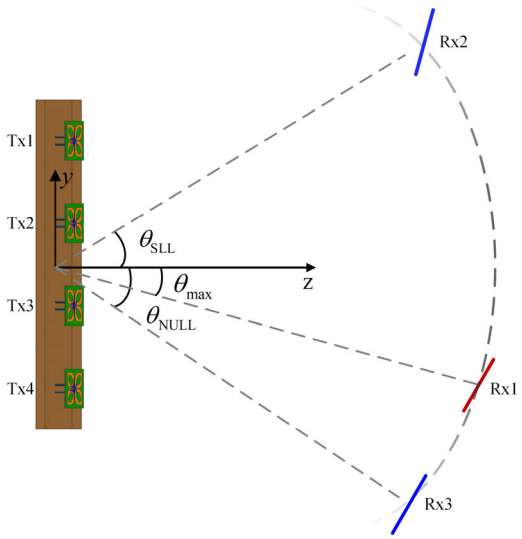

FIGURE 9. Schematic of the WPT system.

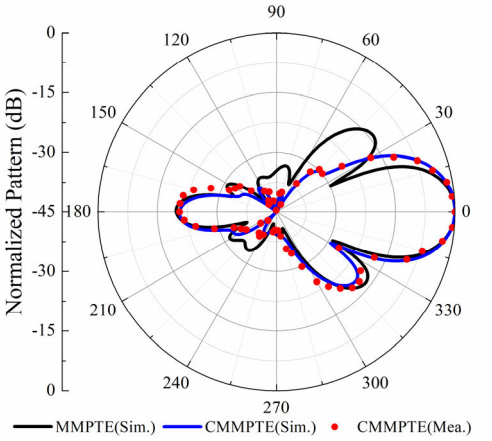

FIGURE 10. Normalized gain pattern with 0° down-tilt angle.

the antenna element and metal reflector. Hence, the beam shaping of the proposed four-element antenna array is carried out in the vertical plane by using the proposed beam shaping scheme. In addition, the antenna array is designed to work in dual polarization states (±45°) so as to increase the signal channel and reliability through the polarization diversity. Due to the symmetry of the antenna array built up with four crossed-dipole elements, only the beams working in +45°-polarization state is shaped by using U-MMPTE and C-MMPTE in LTE and 5G bands.

A. LOW-FREQUENCY BEAMFORMING RESULTS

To obtain the desired shaped beams that operate in +45° polarization state, the excitation amplitudes and phases of the +45°-polarized dipoles are optimized though two steps, while the −45°-polarized dipoles are matched with 50 Ohm loads.

In the first step, a +45°-polarized dipole working at 2.45GHz is selected at the desired down-tilt angle on a far-field arc of the four-element antenna array, as illustrated in Fig.9. By doing this, the first WPT system can be built up and its PTE is given in Eq. (1). The eigenmatrix in Eq. (1) is made up of the S-parameters between the transmitting and testing antenna that can be extracted through HFSS simulation in advance. When the working environment is too complex, the S-parameters can be extracted by measurement, and they include all the affecting factors of a realistic antenna array. The ODE of shaped beam with a desired down-tilt angle can be obtained from Eq. (2), which is corresponding to the maximum PTE of the first WTP system. However, the sidelobe levels and null points are unconstrained in this step by using U-MMPTE.

In the second step, two additional testing antennas are selected on the same far-field arc in the directions of the first upper sidelobe and first lower point null that has been

TABLE 2. The ODE of the antenna array for different down-tilt angles at 2.45GHz.

Angle	Tx1	Tx3	Tx5	Tx7
0°	0.13∠-88	0.36∠-98	0.36∠-83	0.15∠-77
1°	0.35∠-115	0.29∠-124	0.21∠-114	0.16∠-129
2°	0.35∠-110	0.29∠-121	0.21∠-112	0.16∠-127
3°	0.29∠-113	0.43∠-123	0.18∠-123	0.11∠-141
4°	0.13∠-110	0.26∠-125	0.42∠-136	0.19∠-153
5°	0.27∠-100	0.37∠-116	0.27∠-135	0.09∠-156
6°	0.29∠-97	0.37∠-114	0.26∠-137	0.08∠-166
7°	0.21∠74	0.37∠29	0.22∠18	0.21∠0
8°	0.20∠-90	0.28∠-105	0.37∠-136	0.15∠-176
9°	0.17∠-86	0.27∠-119	0.34∠-133	0.22∠169
10°	0.11∠-73	0.24∠-117	0.39∠-141	0.27∠171
11°	0.08∠-72	0.26∠-112	0.47∠-149	0.19∠168
12°	0.22∠-68	0.36∠-113	0.32∠-146	0.11∠151
13°	0.13∠-54	0.27∠-107	0.44∠-150	0.16∠155
14°	0.13∠-55	0.24∠-106	0.38∠151	0.25∠152
15°	0.25∠-53	0.36∠-109	0.27∠-150	0.12∠145
16°	0.15∠-26	0.34∠-109	0.32∠-160	0.19∠149
17°	0.17∠-34	0.31∠-98	0.37∠-159	0.15∠134
18°	0.16∠-29	0.29∠-96	0.39∠-161	0.16∠128

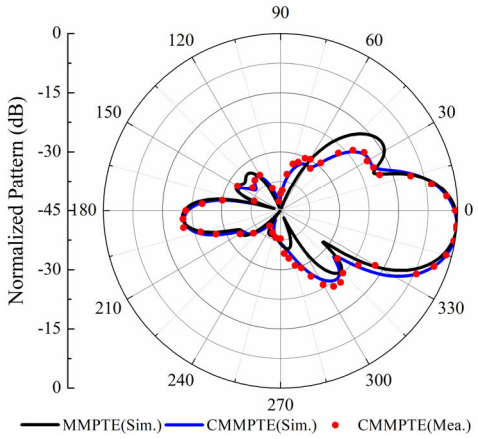

FIGURE 11. Normalized gain pattern with 6° down-tilt angle.

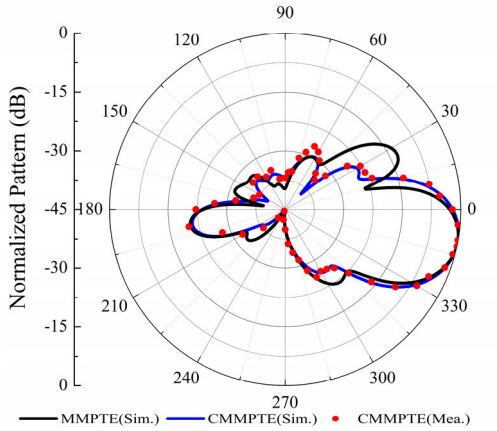

FIGURE 12. Normalized gain pattern with 12° down-tilt angle.

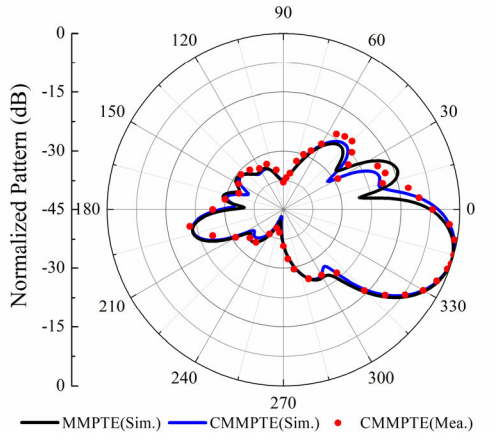

FIGURE 13. Normalized gain pattern with 18° down-tilt angle.

confirmed in the first step. By doing this, the second WPT system is built up. By properly setting up the controlling vector in Eq. (3), the constrained optimization problem can be solved by Eq. (4). For the cellular application of base station, the down-tilt angle is optimized from 0° to 18°, and all the beams are shaped with the constrains of first upper sidelobe level smaller than -18dB, front-to-back ratio larger than 18 dB and filled null point larger than −23 dB. The final ODE is obtained using the C-MMPTE, as listed in Table 2. Such shaped beam constrains satisfy the newest standards for LTE and 5G base stations.

To observe the beam shaping optimized by the U-MMPTE and C-MMPTE, the normalized radiation gain patterns in vertical plane are plotted in Figs. 10-13, where the down-tilt angle are optimized to be 0°, 6°, 12° and 18°, respectively. It can be found that the normalized gain patterns (black line) optimized by U-MMPTE have main beams pointing at the expected down-tilt angles, but the upper sidelobe levels and lower null points are unconstrained. For instance, the first upper sidelobe level is large than −13 dB, and the first lower null point is below −32 dB when the main beam has a 6° down-tilt angle, as shown in Fig.11(black line). In the second step, two additional testing antennas are introduced in the directions of the first upper sidelobe and the first lower null point, and the normalized gain patterns are optimized by C-MMPTE. The normalized gain patterns (blue line) are achieved with suppressed upper sidelobe level, filled-up null point, and keep the down-tilt angle of the main beam unchanged. The constrained normalized gain patterns are measured in a microwave anechoic chamber, which agree well with the simulated results, as shown in Figs.10-13 as well (dot line). Comparing the constrained and unconstrained normalized radiation patterns, the half-power beam width (HPBW) is slightly widened, and all the first upper sidelobe level is suppressed below −16 dB, and the first lower null point is filled up to −23 dB. For instance, the first upper sidelobe level is suppressed to be −23 dB, and the first lower null point is filled up to −20 dB when the main beam has a 6° down-tilt angle, as shown in Fig.11 as well. It should be declared that the cross-polar radiation gain is small enough due to the low cross-polar radiation of the antenna element as shown in Fig.4. Hence, it is not plotted in Fig.10-13. Meanwhile, the front-to-back ratio is larger than 20 dB.

TABLE 3. The ODE of the antenna array for different down-tilt angles at 3.5GHz.

Angle	Tx1	Tx3	Tx5	Tx7
0°	0.10∠154	0.39∠135	0.36∠136	0.14∠154
1°	0.10∠164	0.39∠144	0.37∠145	0.14∠161
2°	0.15∠180	0.36∠154	0.35∠149	0.14∠149
3°	0.11∠180	0.36∠153	0.38∠144	0.15∠141
4°	0.16∠-166	0.35∠159	0.36∠143	0.13∠131
5°	0.14∠-161	0.36∠163	0.41∠141	0.09∠109
6°	0.13∠-160	0.36∠164	0.43∠138	0.08∠102
7°	0.28∠-75	0.40∠-111	0.25∠-149	0.06∠166
8°	0.28∠-71	0.38∠-111	0.26∠-148	0.08∠-156
9°	0.13∠-54	0.27∠-107	0.44∠-150	0.16∠155

B. HIGH-FREQUENCY BEAMFORMING RESULTS

Same beam shaping procedure is executed for the high frequency at 3.5GHz within the lower 5G band. However, the down-tilt angle of the main beam is optimized from 0° to 9° as the larger element spacing at high frequency will cause grating lobe when the main beam points at a large elevation angle. The final ODE obtained by using the proposed beam shaping scheme is listed in Table 3. To observe the shaped beams optimized by using the U-MMPTE and C-MMPTE, the normalized gain patterns in vertical plane are plotted in Figs. 14-16, where the down-tilt angle are chosen to be 0°, 3°, and 9°, respectively. Comparing the constrained and unconstrained radiation patterns, the HPBW remains about 15°, and all the first upper sidelobe levels are suppressed below −19 dB, and all the first lower null points are filled up to −20 dB. Meanwhile, all the front-to-back ratio between the main beam and back lobe level is larger than 22 dB.

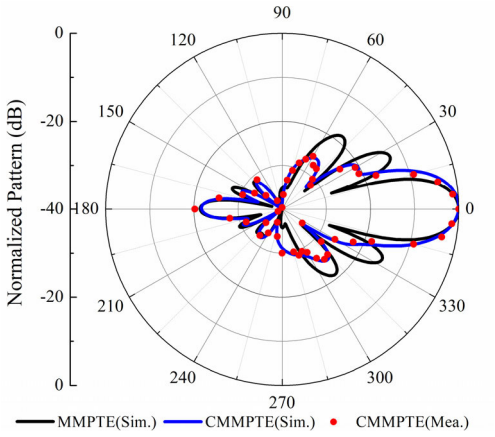

FIGURE 14. Normalized gain pattern with 0° down-tilt angle.

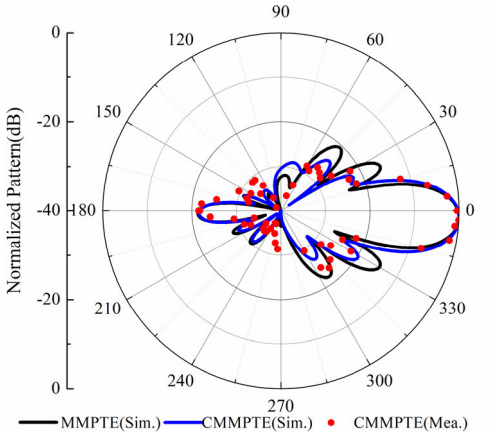

FIGURE 15. Normalized gain pattern with 3° down-tilt angle.

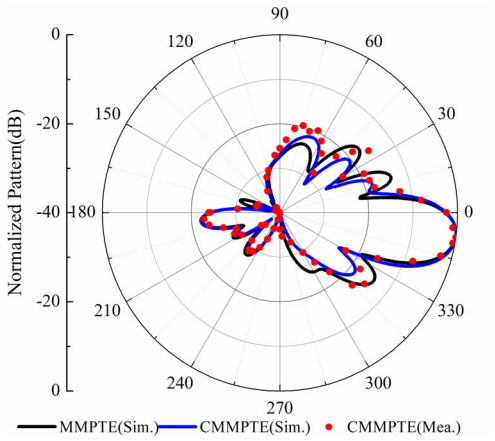

FIGURE 16. Normalized gain pattern with 9° down-tilt angle.

IV. CONCLUSION

In summary, a beam shaping scheme based on the U-MMPTE and C-MMPTE is proposed to the synthesis of the radiation pattern of a dual-band dual-polarized antenna array. The demonstrated cases show that the proposed beam shaping scheme is capable of forming radiation patterns under the constrains of keeping maximum possible gain at the desired down-tilt angle, suppressed sidelobe level, filled-up null point larger, and large front-to-back ratio. In addition, due to the feature of the reported beam shaping scheme, it is applicable to any realistic configuration of the antenna array in any complicated environments.

REFERENCES

[1] Z. D. Zaharis, "Radiation pattern shaping of a mobile base station antenna array using a particle swarm optimization based technique," *Electr. Eng.*, vol. 90, no. 4, pp. 301–311, Apr. 2008.

[2] R. Wu and Q.-X. Chu, "A compact, dual-polarized multiband array for 2G/3G/4G base stations," *IEEE Trans. Antennas Propag.*, vol. 67, no. 4, pp. 2298–2304, Apr. 2019.

[3] Y. Zhu, Y. Chen, and S. Yang, "Decoupling and low-profile design of dual-band dual-polarized base station antennas using frequency-selective surface," *IEEE Trans. Antennas Propag.*, vol. 67, no. 8, pp. 5272–5281, Aug. 2019.

[4] A. Alieldin, "A triple-band dual-polarized indoor base station antenna for 2G, 3G, 4G and sub-6 GHz 5G applications," *IEEE Access*, vol. 6, pp. 49209–49216, 2018.

[5] H.-H. Sun, C. Ding, H. Zhu, B. Jones, and Y. J. Guo, "Suppression of cross-band scattering in multiband antenna arrays," *IEEE Trans. Antennas Propag.*, vol. 67, no. 4, pp. 2379–2389, Apr. 2019.

[6] Y. Gou, S. Yang, J. Li, and Z. Nie, "A compact dual-polarized printed dipole antenna with high isolation for wideband base station applications," *IEEE Trans. Antennas Propag.*, vol. 62, no. 8, pp. 4392–4395, Aug. 2014.

[7] Y. Cui, R. Li, and H. Fu, "A broadband dual-polarized planar antenna for 2G/3G/LTE base stations," *IEEE Trans. Antennas Propag.*, vol. 62, no. 9, pp. 4836–4840, Sep. 2014.

[8] Q. Zhang and Y. Gao, "A compact broadband dual-polarized antenna array for base stations," *IEEE Antennas Wireless Propag. Lett.*, vol. 17, no. 6, pp. 1073–1076, Jun. 2018.

[9] Z. Bao, Z. Nie, and X. Zong, "A novel broadband dual-polarization antenna utilizing strong mutual coupling," *IEEE Trans. Antennas Propag.*, vol. 62, no. 1, pp. 450–454, Jan. 2014.

[10] C. Ding, H. Sun, R. W. Ziolkowski, and Y. J. Guo, "Simplified tightly-coupled cross-dipole arrangement for base station applications," *IEEE Access*, vol. 5, pp. 27491–27503, 2017.

[11] X. Yang, L. Ge, J. Wang, and C.-Y.-D. Sim, "A differentially driven dual-polarized high-gain stacked patch antenna," *IEEE Antennas Wireless Propag. Lett.*, vol. 17, no. 7, pp. 1181–1185, Jul. 2018.

[12] K. M. Mak, X. Gao, and H. W. Lai, "Low cost dual polarized base station element for long term evolution," *IEEE Trans. Antennas Propag.*, vol. 62, no. 11, pp. 5861–5865, Nov. 2014.

[13] R. Lian, Z. Wang, Y. Yin, J. Wu, and X. Song, "Design of a low-profile dual-polarized stepped slot antenna array for base station," *IEEE Antennas Wireless Propag. Lett.*, vol. 15, pp. 362–365, 2016.

[14] Y. Liu, S. Wang, X. Wang, and Y. Jia, "A differentially fed dual-polarized slot antenna with high isolation and low profile for base station application," *IEEE Antennas Wireless Propag. Lett.*, vol. 18, no. 2, pp. 303–307, Feb. 2019.

[15] L.-H. Ye, L. Yuanjun, and D.-L. Wu, "Dual-wideband dual-polarized dipole antenna with T-shaped slots and stable radiation pattern," *IEEE Antennas Wireless Propag. Lett.*, vol. 21, no. 3, pp. 610–614, Mar. 2022.

[16] Q. Xue, S. W. Liao, and J. H. Xu, "A differentially-driven dual-polarized magneto-electric dipole antenna," *IEEE Trans. Antennas Propag.*, vol. 61, no. 1, pp. 425–430, Jan. 2013.

[17] C. Drane Jr., "Dolph–Chebyshev excitation coefficient approximation," *IEEE Trans. Antennas Propag.*, vol. AP-12, no. 6, pp. 781–782, Nov. 1964.

[18] J.-Y. Li, Y.-X. Qi, and S.-G. Zhou, "Shaped beam synthesis based on superposition principle and Taylor method," *IEEE Trans. Antennas Propag.*, vol. 65, no. 11, pp. 6157–6160, Nov. 2017.

[19] K.-K. Yan and Y. Lu, "Sidelobe reduction in array-pattern synthesis using genetic algorithm," *IEEE Trans. Antennas Propag.*, vol. 45, no. 7, pp. 1117–1122, Jul. 1997.

[20] D. Marcano and F. Duran, "Synthesis of antenna arrays using genetic algorithms," *IEEE Antennas Propag. Mag.*, vol. 42, no. 3, pp. 12–20, Jun. 2000.

[21] J. R. Pérez and J. Basterrechea, "Particle-swarm optimization and its application to antenna far-field-pattern prediction from planar scanning," *Microw. Opt. Technol. Lett.*, vol. 44, no. 5, pp. 398–403, Mar. 2005.
[22] Z. Zaharis, D. Kampitaki, P. Lazaridis, A. Papastergiou, A. Hatzigaidas, and P. Gallion, "Improving the radiation characteristics of a base station antenna array using a particle swarm optimizer," *Microw. Opt. Technol. Lett.*, vol. 49, no. 7, pp. 1690–1698, 2007.
[23] B. Fuchs, "Synthesis of sparse arrays with focused or shaped beampattern via sequential convex optimizations," *IEEE Trans. Antennas Propag.*, vol. 60, no. 7, pp. 3499–3503, Jul. 2012.
[24] Q. Lu, G. Cui, R. Liu, and X. Yu, "Beampattern synthesis via first-order iterative convex approximation," *IEEE Antennas Wireless Propag. Lett.*, vol. 20, no. 8, pp. 1493–1497, Aug. 2021.
[25] W. Stutzman, "Synthesis of shaped-beam radiation patterns using the iterative sampling method," *IEEE Trans. Antennas Propag.*, vol. AP-19, no. 1, pp. 36–41, Jan. 1971.
[26] Y.-X. Qi and J.-Y. Li, "Superposition synthesis method for 2-D shaped-beam array antenna," *IEEE Trans. Antennas Propag.*, vol. 66, no. 12, pp. 6950–6957, Dec. 2018.
[27] Z. Chen, F. Liang, Q. Zhang, B. Li, G. Ge, and D. Zhao, "Synthesis method for 1-D uniform microwave field generation based on Fourier transform and time reversal," *IEEE Trans. Antennas Propag.*, vol. 69, no. 10, pp. 7011–7016, Oct. 2021.
[28] Y.-X. Qi and J.-Y. Li, "Difference pattern synthesis based on superposition principle," *IEEE Trans. Antennas Propag.*, vol. 69, no. 5, pp. 3005–3009, May 2021.
[29] W. Geyi, *Foundations for Radio Frequency Engineering*. London, U.K.: World Science, 2015, ch. 5.
[30] S.-Y. Wang, X.-R. Jin, P. Liu, and W. Geyi, "Fast multinull steering of antenna array," *IEEE Antennas Wireless Propag. Lett.*, vol. 21, no. 12, pp. 2512–2516, Dec. 2022.
[31] S.-Y. Wang, K.-X. Zhang, F. Wang, and G.-Y. Wen, "Design of a 360° continuously scanning circular array anttena," *Acta Phys. Sinica*, vol. 71, no. 24, 2022, Art. no. 248402.
[32] X. Cai, X. Gu, and W. Geyi, "Optimal design of antenna arrays focused on multiple targets," *IEEE Trans. Antennas Propag.*, vol. 68, no. 6, pp. 4593–4603, Jun. 2020.
[33] W. Geyi, "The method of maximum power transmission efficiency for the design of antenna arrays," *IEEE Open J. Antennas Propag.*, vol. 2, pp. 412–430, 2021.

LIN GUO was born in Shandong, China, in 1995. She received the B.S. degree in communication engineering from Qingdao Agricultural University, Qingdao, China. She is currently pursuing the M.Eng. degree in information and communication engineering with the Nanjing University of Information Science and Technology, Nanjing, China. Her research interests include RF circuits, base station antennas, and beam-shaping techniques of antenna arrays.

SHEN-YUN WANG (Member, IEEE) was born in Hubei, China, in 1981. He received the Ph.D. degree in information and communication systems from the Nanjing University of Aeronautics and Astronautics, Nanjing, China, in 2012. From 2009 to 2011, he was a Visiting Ph.D. Student with the National University of Singapore, Singapore. He is currently an Associate Professor with the Research Center of Applied Electromagnetics, Nanjing University of Information Science and Technology, Nanjing. His research interests include microwave theory and technology, reconfigurable antennas, array antennas, and electromagnetic compatibility.

GUO-WEN DING (Member, IEEE) received the B.S. degree in electronic information science and engineering and the M.S. degree in electronic and communication engineering from the Nanjing University of Aeronautics and Astronautics, Nanjing, China, in 2013 and 2016, respectively, and the Ph.D. degree in electronic science and engineering from Nanjing University, Nanjing, in 2020. He is currently a Lecturer with the School of Electronic and Information Engineering, Nanjing University of Information Science and Technology, Nanjing. His research interests include microwave theory and technology, reconfigurable antennas, and electromagnetic metamaterials and metasurfaces.

WEN GEYI was born in Pingjiang, Hunan, China, in 1963. He received the B.Eng., M.Eng., and Ph.D. degrees in electrical engineering from Xidian University, Xi'an, China, in 1982, 1984, and 1987, respectively. From 1988 to 1990, he was a Lecturer with Radio Engineering Department, Southeast University, Nanjing, China. From 1990 to 1992, he was an Associate Professor with the Institute of Applied Physics, University of Electronic Science and Technology of China (UESTC), Chengdu, China. From 1992 to 1993, he was a Visiting Researcher with the Department of Electrical and Computer Engineering, University of California at Berkeley, Berkeley, CA, USA. From 1993 to 1998, he was a Full Professor with the Institute of Applied Physics, UESTC. From 1996 to 1997, he was the Vice Chairperson of the Institute of Applied Physics, UESTC, where he was the Chairperson, from 1997 to 1998. From February 1998 to May 1998, he was a Visiting Professor with the Electrical Engineering Department, University of Waterloo, Waterloo, ON, Canada. From 1998 to 2007, he was with Blackberry Ltd., Waterloo, first as a Senior Scientist with the Radio Frequency Department, and then as the Director of Advanced Technology Department. Since 2010, he has been a National Distinguished Professor with Fudan University, Shanghai, China, and the Nanjing University of Information Science and Technology (NUIST), Nanjing. He is currently the Director of the Research Center of Applied Electromagnetics, NUIST. He has authored more than 100 publications and *Foundations for Radio Frequency Engineering* (World Scientific, 2015), *Foundations of Applied Electrodynamics* (Wiley, 2010), *Advanced Electromagnetic Field Theory* (China: National Defense Publishing House, 1999), and *Modern Methods for Electromagnetic Computations* (China: Henan Science and Technology Press, 1994). He holds more than 40 patents. His current research interests include microwave theory and techniques, and antennas and wave propagation.